doi:10.1093/brain/aww003 BRAIN 2016: 139; 1527–1538 | 1527

BRAIN
A JOURNAL OF NEUROLOGY

Network-selective vulnerability of the human cerebellum to Alzheimer's disease and frontotemporal dementia

Christine C. Guo,[1] Rachel Tan,[2,3] John R. Hodges,[2,3,4] Xintao Hu,[5] Saber Sami[6] and Michael Hornberger[2,4,7]

See Schmahmann (doi:10.1093/brain/aww064) for a scientific commentary on this article.

Neurodegenerative diseases are associated with distinct and distributed patterns of atrophy in the cerebral cortex. Emerging evidence suggests that these atrophy patterns resemble intrinsic connectivity networks in the healthy brain, supporting the network-based degeneration framework where neuropathology spreads across connectivity networks. An intriguing yet untested possibility is that the cerebellar circuits, which share extensive connections with the cerebral cortex, could be selectively targeted by major neurodegenerative diseases. Here we examined the structural atrophy in the cerebellum across common types of neurodegenerative diseases, and characterized the functional connectivity patterns of these cerebellar atrophy regions. Our results showed that Alzheimer's disease and frontotemporal dementia are associated with distinct and circumscribed atrophy in the cerebellum. These cerebellar atrophied regions share robust and selective intrinsic connectivity with the atrophied regions in the cerebral cortex. These findings for the first time demonstrated the selective vulnerability of the cerebellum to common neurodegenerative disease, extending the network-based degeneration framework to the cerebellum. Our work also has direct implications on the cerebellar contribution to the cognitive and affective processes that are compromised in neurodegeneration as well as the practice of using the cerebellum as reference region for ligand neuroimaging studies.

1 QIMR Berghofer Medical Research Institute, Herston, Queensland, Australia
2 Neuroscience Research Australia, Sydney, Australia
3 School of Medical Sciences, University of New South Wales, Sydney, Australia
4 ARC Centre of Excellence in Cognition and its Disorders, Sydney, Australia
5 School of Automation, Northwestern Polytechnical University, Xian, China
6 Department of Clinical Neurosciences, University of Cambridge, Cambridge, UK
7 Norwich Medical School, University of East Anglia, Norwich, UK

Correspondence to: Dr Michael Hornberger,
Norwich Medical School,
University of East Anglia,
Norwich, NR4 7TJ,
UK
E-mail: m.hornberger@uea.ac.uk

Keywords: intrinsic connectivity; cerebellum; neurodegeneration; selective vulnerability

Abbreviations: ACE-R = Addenbrooke's Cognitive Examination-Revised; (bv)FTD = (behavioural variant) frontotemporal dementia; CBI-R = Cambridge Behavioural Inventory-Revised; nfv/svPPA = non-fluent variant/semantic variant primary progressive aphasia

Received May 26, 2015. Revised November 9, 2015. Accepted December 6, 2015. Advance Access publication February 16, 2016

Introduction

Common neurodegenerative diseases are associated with progressive and circumscribed atrophy in the cerebral cortex, with distinct anatomical distributions. In Alzheimer's disease, neuropathology predominantly targets the bilateral posterior cingulate cortices, precuneus, and hippocampus, whereas frontotemporal dementia (FTD) affects the frontal and temporal lobes of the brain (Braak and Braak, 1991; Rosen *et al.*, 2002). Importantly, the cerebral atrophy in neurodegeneration have been shown to resemble the anatomical patterns of intrinsic connectivity networks in healthy brains, such as the default mode and salience networks (Greicius *et al.*, 2004; Seeley *et al.*, 2009). As revealed by functional MRI, these networks feature spontaneous, temporally synchronous, spatially distributed neural activities, which presumably result from direct or indirect anatomical connections (Beckmann *et al.*, 2005; Fox *et al.*, 2005; Damoiseaux, 2006; Vincent *et al.*, 2007). The anatomical similarity between the atrophy patterns in neurodegeneration and intrinsic connectivity networks in health provided the first empirical evidence in living humans that neurodegenerative diseases represent organized large-scale network breakdowns and neuropathology spreads along trans-synaptic connections (Seeley *et al.*, 2009). This 'network-based degeneration' framework holds important clinical implications, in elucidating disease-specific profiles and developing imaging markers for diagnosis and disease monitoring.

So far, research on common neurodegenerative diseases has primarily focused on the cerebral cortex. However, connectivity network architecture extends beyond the cerebral cortex, notably, to the cerebellum via topographically-organized connections (Schmahmann, 2001). Structurally, the cerebellum is connected to the cerebral cortex via polysynaptic fibre connections; these connections are organized topographically that different parts of the cerebellum are connected to distinct cerebral regions (Kelly and Strick, 2003; Buckner, 2013). Functionally, most cerebral intrinsic connectivity networks can be mapped onto the cerebellum using functional connectivity analyses (Habas *et al.*, 2009; Buckner *et al.*, 2011). Such topographically-organized connectivity between the cerebrum and the cerebellum led to an intriguing possibility that neurodegeneration could target distinct cerebellar regions within the same intrinsic connectivity network.

Nonetheless, the role of the cerebellum in major neurodegenerative diseases has received little attention. This oversight might be due to the notion that cerebellar degeneration is classically associated with ataxia, a symptoms that is typically absent in Alzheimer's disease and FTD. Recent clinical and neuroimaging studies in human, however, have provided compelling evidence that the cerebellum is broadly involved in cognition, language and emotion (Schmahmann and Sherman, 1998; Schmahmann, 2001; Baumann *et al.*, 2014). Hence, cerebellar changes might not necessarily lead to motor symptoms, but rather compromise cognitive and affective functions. This notion is indirectly corroborated by our recent findings, showing that patients with sporadic behavioural variant FTD have substantial cerebellar changes, particularly in the anterior lobules and the posterior crus (Tan *et al.*, 2014). It is thus an imperative task to characterize pathological changes in the cerebellum accompanying neurodegenerative diseases, and further their relationship with cerebral degeneration.

The current study addresses this issue by systematically mapping the atrophy patterns in the cerebellar and cerebral cortices across four common types of neurodegenerative diseases: Alzheimer's disease and the three FTD subtypes [behavioural variant FTD (bvFTD); semantic dementia (semantic variant primary progressive aphasia, svPPA); progressive non-fluent aphasia (nfvPPA)]. To explore the mechanisms underlying the cerebral atrophy, we mapped the anatomical patterns of cerebellar and cerebral atrophy onto known intrinsic connectivity architecture in healthy brains. Furthermore, we investigated whether the amount of cerebellar atrophy correlated with the cerebral atrophy across patients within each diagnosis group. We hypothesized that (i) different clinical groups would show distinct patterns of cerebellar atrophy; and (ii) the anatomical patterns and the extents of cerebellar and cerebral atrophy within each group would be related as predicted by intrinsic connectivity architecture in healthy brains.

Patients and methods

Case selection

A total of 217 participants took part in this study. Patients were recruited in a consecutive fashion from the FTD Research Clinic, FRONTIER, in Sydney, resulting in a sample of 56 patients with Alzheimer's disease, 38 patients with bvFTD, 30 patients with nfvPPA, 29 patients with svPPA and 64 elderly controls. All FTD patients met current consensus criteria for bvFTD (Rascovsky *et al.*, 2011) and svPPA and nfvPPA (Gorno-Tempini *et al.*, 2011) showing the progressive neuropsychiatric and/or cognitive decline characteristic of this dementia subset. More specifically, patients with bvFTD met criteria for probable bvFTD by showing behavioural disinhibition, apathy, and loss of empathy, as well as a decline in functional abilities. Patients with svPPA had surface dyslexia, as well as impaired naming, single-word comprehension and object knowledge, while having spared repetition and speech production. Patients with nfvPPA had apraxia of speech or agrammatism, as well as complex sentence comprehension problems, while showing intact single-word comprehension and object knowledge. All patients also met criteria of atrophy localized to frontal and/or temporal lobes as well as perisilvian areas via an MRI visual atrophy rating scale (Kipps *et al.*, 2007). Patients with Alzheimer's disease met diagnostic criteria for Alzheimer's disease (Dubois *et al.*, 2007, 2014; McKhann *et al.*, 2011) by having significant episodic memory problems as reported by the patient or carer, which was corroborated by neuropsychological verbal and non-verbal episodic memory

testing (Rey Auditory Verbal Learning Test, Rey figure, Doors and People test) as well as medial temporal lobe atrophy on visual atrophy rating scale (Scheltens *et al.*, 1992). Diagnosis for all patients was established by consensus among a senior neurologist (J.R.H.) and neuropsychologists based on clinical investigations, cognitive assessment, carer interviews, and evidence for atrophy on structural neuroimaging. Patients were excluded when symptom onset was sudden or other significant neurological or psychiatric symptoms were present. No patients were included in the bvFTD group who manifested any amyotrophic lateral sclerosis symptomology or were *C9orf72*-positive. A group of 64 healthy elderly adults were recruited as controls. Testing and scanning was conducted at the first clinic visit of each patient, and patients were followed-up at 12-month intervals for disease management purposes, which also confirmed their additional diagnoses. Based on this database, we selected participants who are best matched for age and gender across the disease and control groups, resulting in the final cohort for this study (34 patients with Alzheimer's disease, 33 patients with bvFTD, 27 patients with nfvPPA, 27 patients with svPPA and 34 control subjects).

Ethics statement

Ethics approval was obtained from the Human Research Ethics Committee of South Eastern Sydney/Illawarra Area Health Service (HREC 10/126, 10/092 and 10/022). Research was conducted following the ethos of the Declaration of Helsinki. Written consent, either from patient or family, was obtained for each participant in the study.

Test selection

The Addenbrooke's Cognitive Examination Revised (ACE-R) and the Cambridge Behavioural Inventory-Revised (CBI-R) were selected on the basis of their high sensitivity, specificity and feasibility for screening cognitive and neuropsychiatric symptoms, respectively.

The ACE-R is a test that detects early cognitive impairment with 94% sensitivity and 89% specificity (Mioshi *et al.*, 2006) and has been well validated across various neurodegenerative diseases. The participant works through a battery of items designed to reveal levels of functioning across five subscales: attention and orientation, memory, fluency, language and visuospatial cognition. The total possible score is 100, with higher scores denoting more preserved cognitive abilities. Scores below 88 are indicative of cognitive impairment (Mioshi *et al.*, 2006).

The CBI-R is a 45-item carer questionnaire mapping the neuropsychiatric topography of the participant and any material impact on daily life. Each item, a given behaviour, is ascribed a frequency rating (0–4): 0, indicating no impairment; 1, a rare occurrence (a few instances per month); 2, a repeated occurrence (a few instances per week); 3, a daily occurrence; and 4, a constant occurrence. The CBI-R stands corroborated by the Neuropsychiatric Inventory (NPI) as an effective measure of neuropsychiatric symptoms (Wedderburn *et al.*, 2008). The maximum score is 180, signifying absolute behavioural and psychological dysfunction (results are reported herein as percentages, for simplicity). Thus higher scores in CBI-R indicate greater impairment, in contrast with grading of ACE-R scores.

Statistical analyses on demographics and neuropsychology

Data were analysed using SPSS19.0 (IBM Corp., Chicago, Ill., USA). Demographic (age, gender, years of education) and clinical (disease duration, FRS Rasch score, ACE-R total score and CBI total scores) variables were checked for normality of distribution by Kolmogorov-Smirnov tests. Variables revealing normal distribution (age, education, FRSRasch) were compared across groups via one-way ANOVAs followed by Bonferroni *post hoc* tests whereas variables with non-normal distributions [gender, disease duration, Clinical Dementia Rating (CDR) sum of boxes, ACE-R total and CBI-R total] were assessed via chi-square, Kruskal-Wallis and Mann-Whitney U-tests.

Imaging acquisition

Subjects were scanned using a 3 T Philips MRI scanner. T_1-weighted acquisition: coronal orientation, matrix 256 × 256 × 200, 1 × 1 mm^2 in-plane resolution, slice thickness 1 mm, echo time/inversion time = 2.6/5.8 ms.

Imaging preprocessing and analysis

T_1-weighted images were segmented into grey and white matter using VBM8 toolbox in SPM8. The output images were visually inspected for each participant to ensure accurate segmentation (see Supplementary Fig. 1 for representative images). The grey matter images were further normalized into Montreal Neurological Institute (MNI) space (affine + non-linear), modulated (non-linear only), and smoothed with an 8 mm full-width at half-maximum Gaussian kernel. These resulting images were subsequently entered into a second-level, random-effects voxel-based morphometry analysis to perform a two sample *t*-test to identify differences between each disease group and healthy controls. The group-difference maps were evaluated with a peak height threshold [family-wise error (FWE)-corrected $P < 0.05$] (Supplementary Fig. 2).

The cerebellum was processed using the spatially unbiased infratentorial template (SUIT) toolbox specifically developed for the cerebellum (Diedrichsen, 2006). Compared with the standard whole-brain atlases, the high resolution atlas used by SUIT preserves the anatomical detail of the cerebellum and provides more accurate spatial registration (Diedrichsen, 2006). The cerebellum was first isolated using a stepwise Bayesian algorithm that estimates the likelihood of each voxel belong to the cerebellum, normalized to the MNI space with the high resolution probability cerebellum template in SUIT (affine + non-linear), modulated, and smoothed with a 2 mm full-width at half-maximum Gaussian kernel. To test whether our results were sensitive to the size of smoothing kernel, 5 mm was also tested. The results were qualitatively similar but less robust and circumscribed (Supplementary Fig. 3). These resulting images were subsequently entered into a second-level, random-effects voxel-based morphometry analysis to perform a two-sample *t*-test to identify between-group differences in the cerebellum. Here, we compared the differences between each of the four disease groups and the healthy controls (four group-comparisons; Fig 1), as well as between the four disease groups (six group-comparisons;

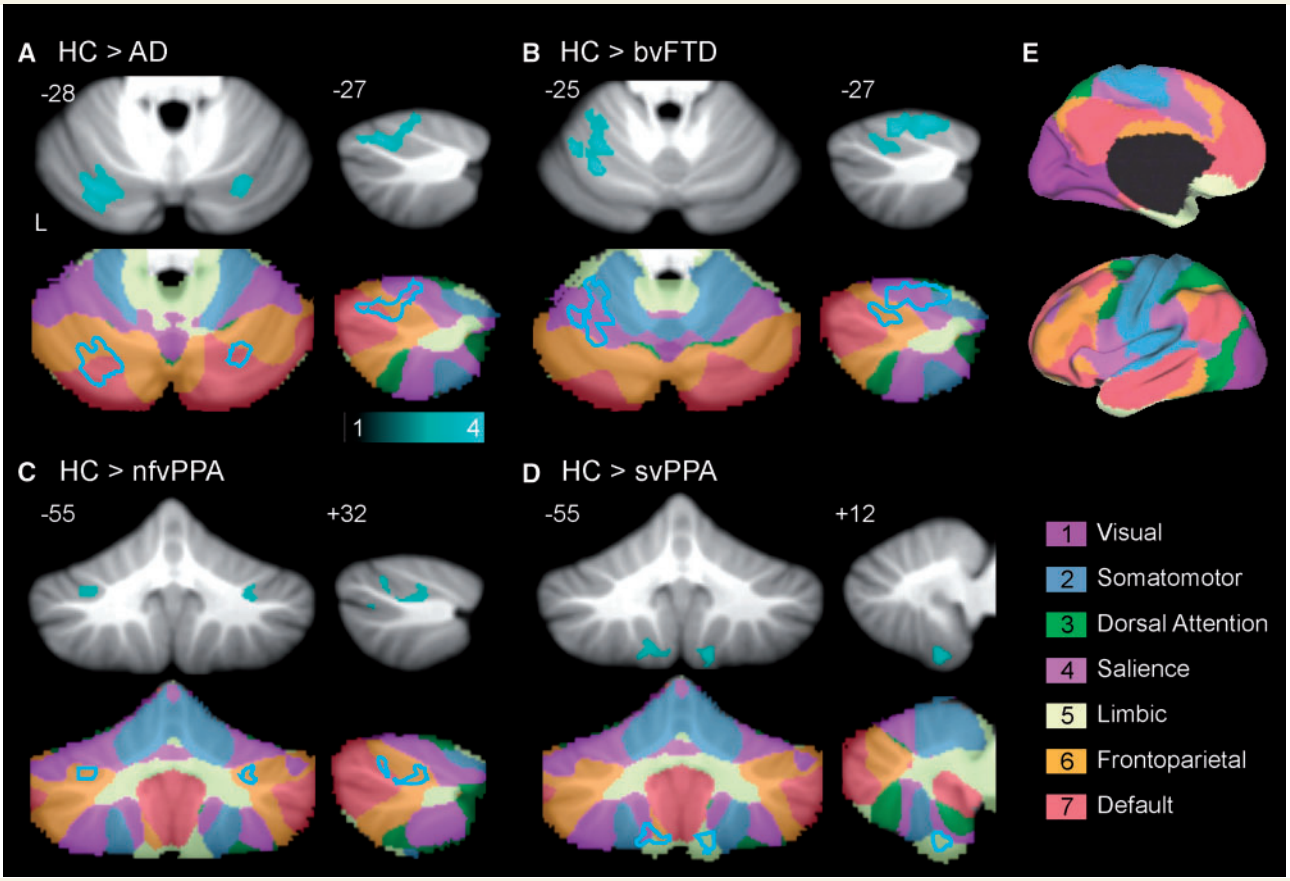

Figure 1 Statistical maps of structural atrophy in the cerebellum in (A) Alzheimer's disease (AD), (B) bvFTD, (C) nfvPPA and (D) svPPA, and their overlays with the Buckner 7-network atlas. (**E**) The corresponding 7-network atlas in the cerebrum (only left hemisphere is shown). $P < 0.001$ (Alzheimer's disease and bvFTD) or 0.005 (nfvPPA and svPPA) for peak height and FWE-corrected $P < 0.05$ for spatial extent. Purple regions in the cerebellum are all part of the salience network, as the visual network, colour-coded as dark purple, does not have a cerebellar counterpart (Buckner *et al.*, 2011). HC = healthy control.

Supplementary Fig. 4). Group-differences in the cerebellum were not detected at the threshold used for the cerebrum (FWE-corrected $P < 0.05$). Hence, a more lenient threshold was used: a peak height threshold ($P < 0.001$ or $P < 0.005$), and cluster extend (FWE-corrected $P < 0.05$).

Age and gender were included as covariates in all group comparisons. As total grey matter or total intracranial volume were corrected during the preprocessing step 'modulation – non-linear only' in VBM8 and SUIT. Note the modulation step (to correct for local expansion or contraction) was implemented by dividing the partial volume maps by the Jacobian of the warp field, therefore correcting for global brain size differences. Total intracranial volume was therefore not included as a covariate in the statistical model. Disease severity as quantified by FRS was included as an additional covariate in all comparisons between disease groups.

These group difference maps were then compared with each of the intrinsic connectivity networks as defined in the Yeo and the Buckner atlas for the cerebrum and the cerebellum, respectively (Buckner *et al.*, 2011; Yeo *et al.*, 2011); the spatial similarity was assessed by goodness-of-fit scores (GOF) according to the following formula, and summarized in Table 2.

$$\mathrm{GOF} = (V_{in} - V_{out})/(V_{in} + V_{out}) \quad (1)$$

where: V_{in} = probability of voxels in the group-difference map to be inside of the connectivity network; and V_{out}: Probability of voxels in the group-difference map to be outside of the connectivity network.

Permutation tests were used to test whether the goodness-of-fit scores of the top-matching network are significantly higher than the rest. Here, group comparisons were performed on randomly-selected subsets of 20 patients to derive the goodness-of-fit scores. This process was repeated 50 times for each disease group and statistical significance between the top and second ranking networks was examined with Mann-Whitney U Test (Table 2).

Seed-based functional connectivity

For each type of neurodegenerative diseases, we selected the peak atrophy regions within the relevant networks in the cerebral and the cerebellar cortex for Alzheimer's disease, bvFTD, nfvPPA and svPPA, respectively (Table 3). As the result, the cluster peaks of group difference maps at the left angular

gyrus, the right anterior insula, the left inferior frontal gyrus and the left inferior temporal gyrus were used as the cerebral seeds, whereas the peaks of group difference maps at the left Crus I, the left VI, the right Crus I and the left IV–V were used as the cerebral seeds, for Alzheimer's disease, bvFTD, nfvPPA and svPPA, respectively.

The intrinsic connectivity of these seeds was examined using resting state functional MRI data from 468 'related' Q1–Q6 subjects (R468), acquired by the human connectome project (WU-Minn HCP Data – 500 Subjects; age 22–35 and 59% female). The preprocessing pipeline of HCP resting state dataset has been described in details in the original publication (Glasser *et al.*, 2013; Smith *et al.*, 2013). Briefly, structural images were corrected for magnetic resonance gradient non-linearity distortion, and registered to the MNI space using an initial linear (FLIRT) and non-linear (FNIRT) registration in FSL. Functional images were corrected for spatial distortions, re-aligned to compensate for subject motion, co-registered to the structural images, smoothed with 2 mm full-width at half-maximum and mapped onto the standard space. The output is a standard set of time series in every subject, with spatial correspondence of 2 mm average surface vertex and subcortical volume voxel spacing. Lastly, FIX (FMRIB's ICA-based X-noisifier) was applied to this set of time series to remove non-neural artefact signals (Smith *et al.*, 2013). FIX combines independent component analysis and hierarchical fusion of classifier to identify spatiotemporal components that mostly reflect artefacts in the data; commonly used noise regressors, such as white matter and CSF time series, were included to assist classification (Salimi-Khorshidi *et al.*, 2014). The time series of identified noise components, as well as the 24 confound time series derived from the motion estimation, were subsequently removed from the functional MRI data; 24 motion-related time series include the six rigid-body parameter time series, their backwards-looking temporal derivatives, plus all 12 resulting regressors squared (Satterthwaite *et al.*, 2013; Smith *et al.*, 2013).

The use of nuisance signal regression is still an outstanding issue for connectivity analyses (Smith *et al.*, 2013). To ensure our results are not sensitive to the choice of this preprocessing step, we examined functional connectivity either with or without additional regressions. Using the workbench 1.0 software, seed-based functional connectivity maps were generated for each of the 468 subjects, based on (i) correlation with regression of the mean grey time course (MGT); and (ii) full correlation between the seeds and every other voxels in the brain (Smith *et al.*, 2013). The regression of MGT, the average time course of grey matter voxels and vertices, represents a less aggressive form of global signal regression (Smith *et al.*, 2013). Then, group-level statistical analyses were performed on the 468 individual functional connectivity maps to derive the intrinsic connectivity networks. The spatial similarity between these intrinsic connectivity networks were then measured by (Pearson) spatial cross-correlation. As the results from the two connectivity maps were quantitatively similar (Table 3), only the MGT-regressed connectivity maps are displayed in the 'Results' section (Fig. 2).

Structural correlation between the cerebral and cerebellar seed regions

To assess the atrophy at the peak atrophy regions that were used as the seeds in the preceding analyse, we created 6-mm sphere regions of interest that were centred at the peak coordinates (Table 3, grey rows). The mean grey matter volumes of these regions of interest were extracted from the structural image of each patient. The associations between the cerebral and cerebellar regions of interest were examined via (Pearson) correlation. One-tailed tests were used, as we had prior hypotheses that the atrophy severity of the cerebral and cerebellar regions of interest within the same, targeted networks would be positively correlated. *Post hoc* residual normality tests were performed on these correlation analyses in SPSS. In all cases, the residuals conformed to a Gaussian distribution and no outlier was detected.

Results

Demographics and clinical profiles

To establish the atrophy profiles across several common neurodegenerative syndromes, we screened our clinical

Table 1 Demographics and clinical profiles

	Alzheimer's disease ($n = 34$)	bvFTD ($n = 33$)	nfvPPA ($n = 27$)	svPPA ($n = 27$)	Controls ($n = 34$)
Gender (M:F)	19: 15	19: 14	11: 16	18:9	16:18
Age (years)	62 ± 6	61 ± 7[f]	67 ± 10	61 ± 5[f]	64 ± 5
Education (years)	13 ± 3	12 ± 3[a]	13 ± 3	12 ± 3	13 ± 3
Disease duration (years)	3 ± 3	3 ± 2	3 ± 2	4 ± 3[c,f]	N/A
CDR	3.9 ± 2.2	6.4 ± 3.6[d]	1.9 ± 2.1[d,e]	3.3 ± 2.7[e,f]	N/A
FRS Rasch score	1.0 ± 1.4[e]	0.6 ± 0.5	0.4 ± 0.5[e]	1.5 ± 1.3[e,d,f]	N/A
ACE-R Total	67.2 ± 18.0[b]	76.7 ± 11.7[b,c]	76.5 ± 14.8[b,c]	61.6 ± 18.2[b,c,e,g]	95.4 ± 3.4
CBI Total	21.7 ± 13.4 [b]	37.1 ± 15.8[b,d]	12.4 ± 11.0[b,d,e]	25.6 ± 16.7[b,e,g]	3.0 ± 2.9

[a]$P < 0.05$ compared to controls.
[b]$P < 0.01$ compared to controls.
[c]$P < 0.05$ compared to Alzheimer's disease.
[d]$P < 0.01$ compared to Alzheimer's disease.
[e]$P < 0.01$ compared to bvFTD.
[f]$P < 0.05$ compared to nfvPPA.
[g]$P < 0.01$ compared to nfvPPA.

Table 2 Goodness-of-fit scores between atrophy patterns and top two best-matching intrinsic connectivity networks

	Alzheimer's disease		bvFTD		nfvPPA		svPPA	
	#ICN	GOF	#ICN	GOF	#ICN	GOF	#ICN	GOF
7-Network parcellation								
Cerebellum								
No. 1	7**	0.47	4**	0.44	6*	0.56	2**	0.42
No. 2	6	0.32	2	0.16	7	0.34	5	0.23
Cerebrum								
No. 1	7**	0.56	4**	0.54	6**	0.66	5**	0.86
No. 2	3	0.32	7	0.40	4	0.51	7	0.11
17-Network parcellation								
Cerebellum								
No. 1	17*	0.57	8*	0.46	17**	0.78	15	0.70
No. 2	14	0.47	13	0.37	8	0.20	11	0.68
Cerebrum								
No. 1	17**	0.65	8**	0.65	12*	0.81	9**	0.91
No. 2	14	0.53	10	0.45	8	0.63	17	0.53

To avoid naming confusions, intrinsic connectivity networks (ICNs) are labelled here by the numbers used in the original atlas. For the visual displays of these networks, see Fig. 1E for the 7-network parcellation atlas, and Fig. 11A in Buckner *et al.* (2011) for the 17-network parcellation atlas. The 7 network: 1, Visual; 2, Somatosensory; 3, Dorsal attention; 4, Salience; 5, Limbic; 6, Frontoparietal; 7, Default. The 17 network: 1, 2, Visual; 3, 4, Somatosensory; 5, 6, Dorsal attention; 7, 8, Salience; 9, 10, Limbic; 11–13, Frontoparietal; 14–17, Default. Networks that match significantly better than the rest are signified with $^{**}P < 0.001$ and $^{*}P < 0.01$. GOF = goodness-of-fit.

Table 3 Cross correlation between the cerebral and cerebellar peak atrophy regions seeded intrinsic connectivity networks

		Cerebral			
		Alzheimer's disease L AG	BvFTD R AI	NfvPPA L IFG	SvPPA L ITL
Cerebellar	Alzheimer's disease L CRUS I	0.61/0.51	−0.34/−0.04	0.37/−0.03	0.06/−0.14
	BvFTD L VI	−0.34/0.23	0.57/0.73	0.16/0.27	−0.36/−0.32
	NfvPPA R CRUS I	0.36/0.36	−0.16/0.25	0.60/0.46	−0.19/−0.17
	SvPPA L IV–V	0.29/0.36	−0.13/0.19	0.00/0.12	0.08/0.18

Results are shown for both connectivity measures: correlation with mean grey time course (MGT) regression/functional correlation.

database for patients diagnosed with Alzheimer's disease, bvFTD, svPPA and nfvPPA, and healthy controls, who are best matched for age and gender (Table 1). The resultant four groups have no significant difference in gender or years of education ($P > 0.1$ for all). Age was not significantly different between most groups ($P > 0.1$), except that the nfvPPA group showed significantly older age as compared to the bvFTD and svPPA groups ($P < 0.05$). As the nfvPPA group did not differ from the control group in age, we opted to include all patients, rather than exclude the older ones and reduce the sample size. A longer disease duration was found in svPPA compared to Alzheimer's disease and nfvPPA ($P < 0.05$) but no other difference was found across groups. On the CDR assessments, patients with nfvPPA scored higher than all patient groups ($P < 0.05$) and patients with bvFTD scored significantly worse in comparison to Alzheimer's disease and svPPA ($P < 0.01$). As expected, all patient groups performed significantly worse in comparison to controls in ACE-R and CBI assessments ($P < 0$ .01). For the ACE-R, svPPA cases performed worse in comparison to all other groups ($P < 0.05$ for all). A poorer performance was also seen in Alzheimer's disease and nfvPPA compared to bvFTD ($P < 0.05$). For the CBI scores, the svPPA cohort performed significantly worse in comparison to nfvPPA ($P < 0.01$) but both svPPA and nfvPPA cohorts performed significantly better in comparison to behavioural variant FTD cases ($P < 0.01$), with nfvPPA also performing better in comparison to Alzheimer's disease ($P < 0.01$). Significant differences were seen in the FRS Rasch score in Alzheimer's

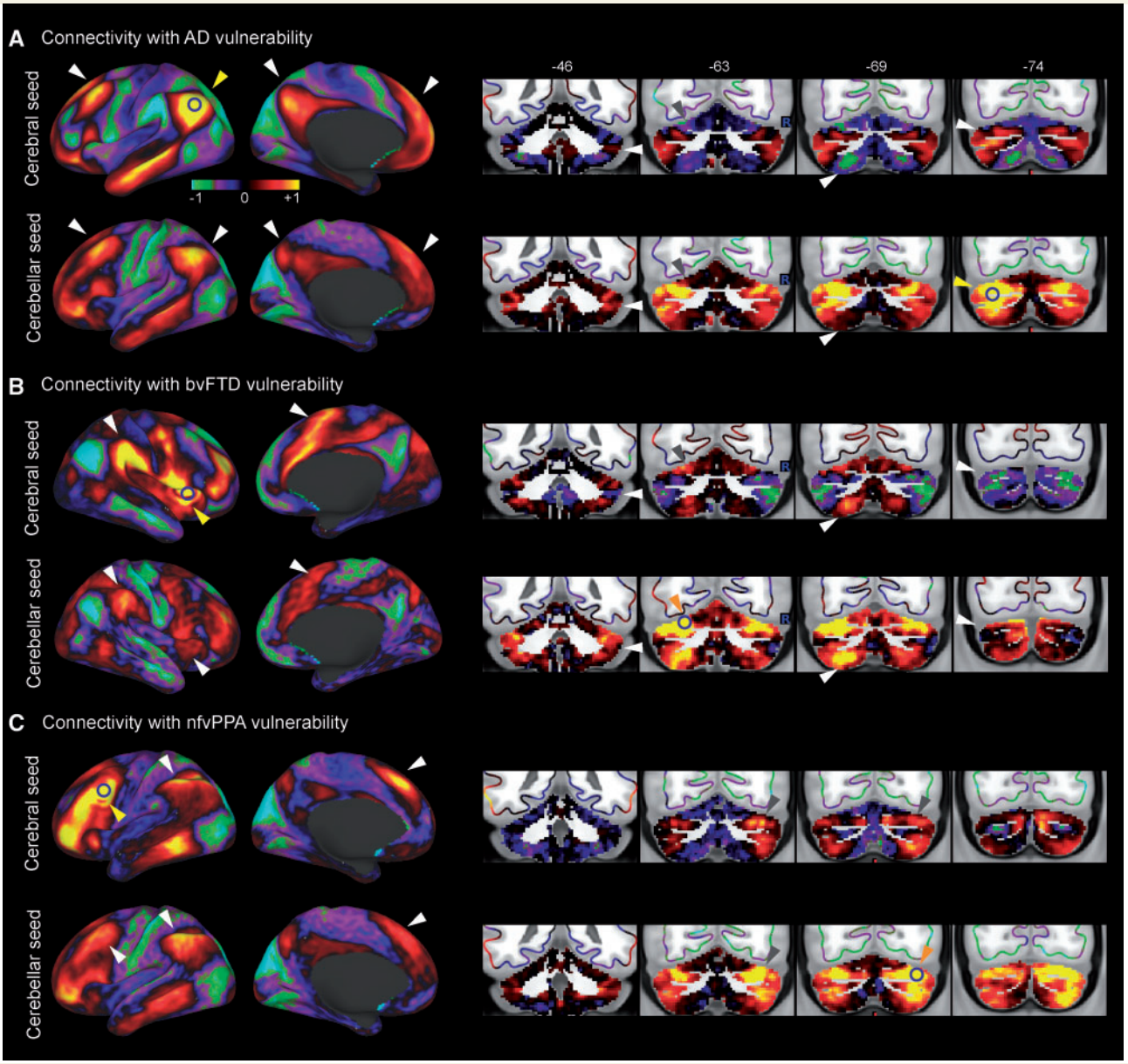

Figure 2 Intrinsic connectivity patterns of cerebral (*top row*) and cerebellar (*bottom row*) atrophy regions in Alzheimer's disease (A) and bvFTD (B). Seed regions are signified by yellow arrowhead. Additional anatomical landmarks are signified by white/grey arrowheads to assist visual inspection.

disease, svPPA and nfvPPA in comparison to bvFTD ($P < 0.01$) as well as in svPPA compared to Alzheimer's disease and nfvPPA ($P < 0.05$).

Distinctive patterns of cerebellar atrophy in the Alzheimer's disease and frontotemporal dementia

Alzheimer's disease and FTD subtypes are associated with significant and anatomically-distinct atrophy in the cerebellum. Compared to age-matched healthy controls, patients with Alzheimer's disease showed significant atrophy in the bilateral Crus I (Fig. 1A and Supplementary Table 1; $P <$ 0.001 for voxel height, FWE-corrected $P < 0.05$ for cluster extent). On the other hand, the cerebellar atrophy in behavioural variant FTD was located at the anterior and superior portion of the cerebellum, with peak atrophied regions in lobule VI, predominantly on the left (Fig. 1B and Supplementary Table 1; $P < 0.001$ for voxel height, FWE-corrected $P < 0.05$ for cluster extent). In svPPA and nfvPPA groups, the threshold used above did not detect cerebellar atrophy. A lenient statistical threshold for voxel height ($P < 0.005$) revealed bilateral atrophy in lobules IV–V and IX in svPPA, and Crus I in nfvPPA (Fig. 1C, D and Supplementary Table 1, FWE-corrected $P < 0.05$ for cluster extend). Next, we examined whether the

cerebellar changes are different between these common neurodegenerative disorders. We found the cerebellar atrophy was more severe in Alzheimer's disease than FTD subtypes (Supplementary Fig. 4; FWE-corrected $P < 0.05$ for cluster extent). Specifically, patients with Alzheimer's disease presented greater atrophy in the right and left Crus I than patients with behavioural variant FTD and nfvPPA, respectively. On the other hand, no cerebellar regions were found to show greater atrophy in FTD subtypes than Alzheimer's disease. In addition, no significant differences in the cerebellar cortex were identified between the three FTD subtypes.

Cerebellar atrophy patterns reflect cerebro-cerebellar intrinsic connectivity

If the cerebellar atrophy in neurodegenerative diseases results from the spread of neuropathology across interlinked networks, these atrophied regions in the cerebellum should belong to the same large-scale intrinsic connectivity networks as the corresponding cerebral atrophied regions. To test this hypothesis, we compared the atrophy maps against established cerebral and cerebellar atlas based on resting state connectivity (Buckner *et al.*, 2011; Yeo *et al.*, 2011). It has been well recognized that the cerebral atrophy patterns in Alzheimer's disease and behavioural variant FTD resemble the default mode network anchored by bilateral angular gyrus, precuneus and posterior cingulate cortex, and the salience network anchored by bilateral anterior insula and anterior cingulate cortex, respectively (Greicius *et al.*, 2004; Seeley *et al.*, 2009) (Supplementary Fig. 2). Consistent with these previous findings, the cerebral atrophy patterns in Alzheimer's disease and bvFTD showed the highest matching scores with the default mode network and salience network in the connectivity network atlas, respectively (Table 2 and Supplementary Fig. 2). When we applied a similar analysis in the cerebellum, the cerebellar atrophy pattern matched the best with the cerebellar counterparts of the default mode network and salience network, respectively (Figs. 1A and B, overlaid on the 7-network atlas; Table 2), suggesting that the neurodegeneration in Alzheimer's disease and bvFTD follows large-scale cerebro-cerebellar intrinsic connectivity patterns as identified in healthy brains.

The intrinsic connectivity networks underlying cerebral atrophy are less studied and established for nfvPPA and svPPA (Seeley *et al.*, 2009; Farb *et al.*, 2013; Guo *et al.*, 2013; La Joie *et al.*, 2013). Nonetheless, we observed a similar pattern in nfvPPA, where the atrophied areas best matched the same intrinsic connectivity networks, the frontoparietal network, in both the cerebrum and the cerebellum (Fig. 1C and Table 2). For svPPA, although the limbic network shares high spatial similarity with the cerebral atrophy pattern, its matching with the cerebellar atrophy pattern was poor, suggesting the neurodegenerative process in svPPA might follow different mechanisms between the two brain regions (Fig. 1D and Table 2).

Shared intrinsic connectivity patterns between cerebral and cerebellar atrophy regions

To further validate the cerebro-cerebellar connectivity-based degeneration hypothesis, we adopted a seed-based analytical strategy commonly used in the cerebrum (Seeley *et al.*, 2007; Zhou *et al.*, 2012; Guo *et al.*, 2013). We examined whether the peak atrophied regions in the cerebral and the cerebellar cortices share similar intrinsic connectivity patterns in healthy brains (see 'Patients and methods' section for details; Table 3).

Intrinsic connectivity network seeded at the left angular gyrus, the peak cerebral atrophy region in Alzheimer's disease (Fig. 2A), encapsulates bilateral angular gyrus, middle temporal gyrus, precuneus and dorsal medial prefrontal cortex (dmPFC). Additional, Crus I and II in the cerebellum also showed high connectivity to the angular gyrus seed (Fig. 2A). Intriguingly, the network seeded at left Crus I, the peak cerebellar atrophy region in Alzheimer's disease, resembles this angular gyrus-seeded network, with bilateral angular gyrus, middle temporal gyrus, precuneurs and dmPFC being the most connected cerebral regions (Fig. 2A and Table 3, spatial cross-correlation = 0.61). Similarly, seeding either in the cerebrum or the cerebellum, peak atrophy regions in behavioural variant FTD generated networks encompassing anterior cingulate cortex, bilateral anterior insula, temporoparietal junction, as well as lobules VI and VIII (Fig. 2B and Table 3, spatial cross-correlation = 0.57); peak atrophy regions in nfvPPA show robust, shared connectivity in inferior frontal gyrus, intraparietal sulcus, dmPFC, as well as Crus I and lobule VIII (Table 3, cross-correlation = 0.60). In svPPA, however, cerebral and cerebellar atrophy regions appeared to have different intrinsic connectivity patterns (Table 3, cross-correlation = 0.08).

Correlated cerebral and cerebellar atrophy within the relevant connectivity networks

Finally, based on the network-based generation framework, the severity of degeneration should be correlated between the cerebrum and the cerebellum within the same connectivity networks. We tested this hypothesis with correlational analyses on structural atrophy. In Alzheimer's disease, grey matter volume at the peak atrophy region in Crus I was significantly correlated with grey matter volume at the angular gyrus ($r = 0.38$, $P = 0.01$), but not the anterior insula ($r = 0.08$, $P = 0.32$; Fig. 3A). On the other hand, in bvFTD, grey matter volume at the peak atrophy region in lobule VI was significantly correlated with grey matter volume at the anterior insula ($r = 0.34$, $P = 0.02$), but not the angular

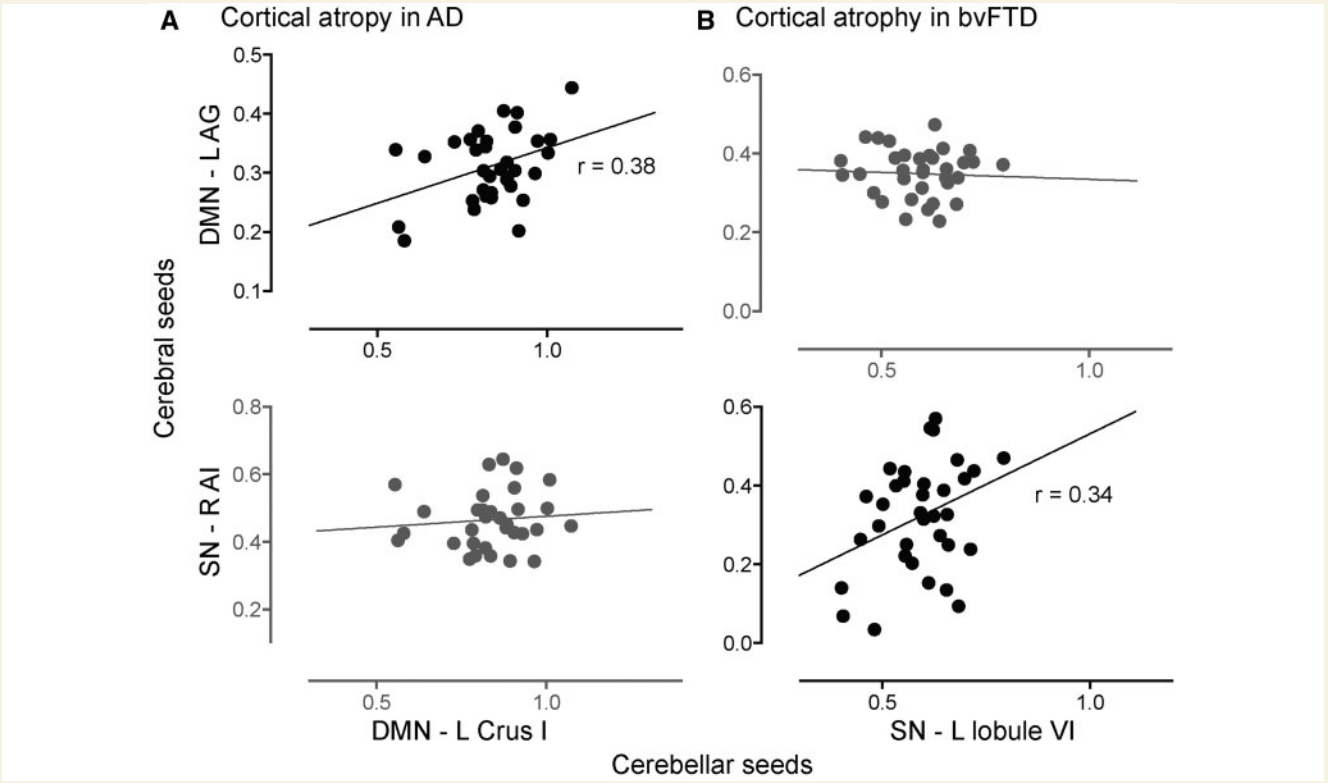

Figure 3 Correlation between cerebral and cerebellar atrophy in patients with Alzheimer's disease (A, AD) and behavioural variant FTD (B). Grey matter volumes from the cerebral and cerebellar seed regions for the default mode network and salience network are plotted against each other. Significant correlations (Bonferroni-corrected for multiple comparisons) are plotted in black and non-significant correlations are plotted in grey.

gyrus ($r = -0.05$, $P = 0.38$; Fig. 3B). We did not find significant correlation between the cerebral and the cerebellar atrophy severity in nfvPPA and svPPA, although there was a trend in nfvPPA ($P = 0.06$).

Discussion

Our findings showed that neurodegenerative syndromes are associated with distinct patterns of atrophy in the cerebellum. These cerebellar atrophy regions shared robust intrinsic connectivity with the atrophy regions in the cerebral cortex, as revealed by seed-based functional connectivity analyses on healthy brains. These results suggested that the network-selective vulnerability could underlie the pathogenesis of neurodegeneration in both the cerebral and cerebellar cortices. We report here that the cerebellar subregions targeted by Alzheimer's disease are within the Crus I/II, and the ones by bvFTD are within lobule VI. Previous studies in healthy adults have classified Crus I/II and lobule VI as the cerebellar counterparts of the default mode network and the salience network, respectively (Habas *et al.*, 2009; Krienen and Buckner, 2009; Buckner *et al.*, 2011). Hence, our observations are consistent with previous research on the cerebral cortex that Alzheimer's disease targets the default mode network and bvFTD targets the salience network (Seeley *et al.*, 2009; Zhou *et al.*, 2010). These results provide strong support that neurodegenerative processes spread across intrinsic connectivity networks in the brain, and further extend this network-based framework to the cerebellum.

To our knowledge, our study is the first to systematically examine cerebellar atrophy in relation to intrinsic brain networks across common neurodegenerative diseases. The cerebellum is generally regarded as being spared in Alzheimer's disease—often serving as a control tissue or a reference region in imaging studies (Smith *et al.*, 1997; Dukart *et al.*, 2010). However, pathological insults in the cerebellum have been widely reported in Alzheimer's disease by earlier pathology studies (Braak *et al.*, 1989; Joachim *et al.*, 1989; Dickson *et al.*, 1990; Mattiace *et al.*, 1990; Fukutani *et al.*, 1996; Ishii *et al.*, 1997; Wegiel *et al.*, 1999; Chen *et al.*, 2010), which oddly became scanty in the more recent literature. On the other hand, the importance of the cerebellum is gaining increasing traction in the field of FTD, fuelled by studies that have found structural changes and neuropathological lesions in the cerebellum in patients carrying the *C9orf72* mutation (Mahoney *et al.*, 2012; Whitwell *et al.*, 2012). The cerebellar changes do not appear to be specific to *C9orf72* mutation though; they

have since been documented in cohorts of sporadic behavioural variant FTD, particularly in the anterior lobules and the crus (Tan *et al.*, 2014), similar to our connectivity results. These findings clearly suggest that caution is warranted to regard the cerebellum as a control or reference region in neurodegenerative conditions, as atrophy in the regions emerges as much more pervasive as previously thought. Future studies should address the impact of those cerebellar changes on ligand neuroimaging and how this can be accounted to avoid biased results.

More importantly, our results demonstrate how network-based framework has become a powerful framework for understanding the mechanisms of neurodegeneration. Not only on a systems level where the anatomical distributions of cerebral atrophy in neurodegenerative diseases resemble intrinsic connectivity networks in healthy brains (Seeley *et al.*, 2009), but also on a molecular level where pathogenic proteins (e.g. amyloid, tau, TDP-43) could misfold and aggregate into self-propagating agents for the spread of disease (Jucker and Walker, 2013). Hence, evidence is converging that the connectivity-based, network-specific mechanisms underlie the origin and progression of neurodegenerative diseases. Under this network-based framework, involvement of the cerebellum should be no surprise. Earlier tracing studies have well documented the topographically-organized connections between the cerebellum and the cerebrum, including prefrontal cortex, via the cerebro-cerebellar-thalamo circuits (Haines and Dietrichs, 1984; Siwek and Pandya, 1991; Haines *et al.*, 1997). Recent functional neuroimaging studies further mapped functional connectivity networks in the cerebral cortex onto distinct cerebellar regions (Habas *et al.*, 2009; Buckner *et al.*, 2011). Together with these structural and functional studies, our results underscore the importance of dissecting the anatomical subdivisions of the cerebellum in elucidating its function and vulnerability to neuropathology. Furthermore, other subcortical structures strongly connecting to the targeted cerebral regions could potentially be vulnerable to neurodegeneration. For example, there has been increasing evidence that the basal ganglia contribute to symptomology in neurodegeneration along with the cortical changes (Shepherd, 2013). Future study could take a similar approach for the whole brain to establish a complete depiction of neural network changes in neurodegeneration.

This cerebro-cerebellar connectivity is critical for the understanding the clinical pathological correlates in neurodegenerative diseases. Indeed, historically the cerebellum has been associated with coordination and motor symptoms. However, more recent evidence suggests that somatosensory regions occupy only a relatively small proportion of the cerebellum, with almost one-half of the cerebellum involved in cognitive control and the default mode networks (Buckner *et al.*, 2011). Functional imaging studies have highlighted the role of Crus I in working memory and connectivity studies have corroborated this by demonstrating that the cerebellar Crus I/II are the major cerebellar regions coupled to the default network (Krienen and Buckner, 2009; Buckner *et al.*, 2011). The current study shows peak atrophy in Crus I being associated with the default mode network targeted in Alzheimer's disease, and the cerebellar lobule VI with the salience network in bvFTD. The presence of cerebellar degeneration raises intriguing questions on the cerebellar contribution to the cognitive and affective symptoms in these patients, who have no or very subtle motor symptoms. More likely, if taken an integrative view of the brain function, the integrity of the entire circuit, that encompasses the relevant cerebral and cerebellar cortices, as well as subcortical structures, is the key to support healthy mental states. This is clearly speculation at this stage, and future studies addressing these issues are evidently needed.

Despite these significant findings in Alzheimer's disease and bvFTD, results for the nfvPPA and svPPA groups were less robust. Indeed, a more lenient threshold was needed to detect cerebellar atrophy in nfvPPA and svPPA (Fig. 1). The weaker statistical significance could be due to the smaller sample sizes of the nfvPPA and svPPA groups. Alternatively, it might reflect that the cerebellum is less affected in nfvPPA and svPPA than Alzheimer's disease and behavioural variant FTD, although a direct comparison of FTD subtypes did not show significant differences (Supplementary Fig. 4). One could speculate that the observed differences could be due to stronger anatomical connections between the cerebrum and the cerebellum, which might lead to a higher susceptibility of cerebellar atrophy. Clearly this anatomical connectivity needs to be further investigated. In Alzheimer's disease and behavioural variant FTD, atrophy in strongly connected cortical regions such as the parietal and prefrontal cortices might cause greater cerebellar atrophy, leading to the clear relationship between cerebellar atrophy and connectivity. On the other hand, the anterior temporal lobe, the targeted cerebral regions in svPPA, might not share strong connections with the cerebellum, resulting in a much weaker relationship. This possibility, however, remains a speculation; investigations of the cerebellar changes in the language variant, particularly svPPA, are warranted in future studies employing bigger sample sizes.

Limitations and future directions

Despite these promising findings there were several limitations to our findings. The effects of cerebellar atrophy as measured by structural MRI were moderate in our study, compared to the atrophy in the cerebrum. This moderate effect, however, might not necessarily reflect the degree of cerebellar atrophy or pathology in Alzheimer's disease and FTD. Standard structural MRI technique could be suboptimal for measuring the structure of the cerebellum due to its high neuronal density. The human cerebellum contains more than half of all the neurons within the brain within $<10\%$ of its volume, resulting in the densely-packed and highly-convoluted cerebellar cortex. Hence, future studies

using high-resolution structural MRI and functional MRI could provide valuable insights into the structural and functional vulnerability of the cerebellum and other subcortical structures in much finer details. High-resolution neuroimaging could also enhance the ability to investigate the relationship between the degenerative processes in the cerebrum and the cerebellum. Our results provide preliminary evidence that the severity of cerebral and cerebellar atrophy are selectively correlated within the same intrinsic connectivity networks (Fig. 3). However, the correlations we detected were only moderate ($r = 0.3 \sim 0.4$). To fully address this notion of co-atrophy, these analyses should be further investigated by neuroimaging studies that offer improved spatial resolution and account for other confounding factors. Finally, our study did not address the contribution of cerebellar lesion to clinical profiles in Alzheimer's disease and FTD and did not allow us to confirm the findings in pathologically confirmed cases. Future studies combining high-resolution cerebellum imaging and comprehensive neuropsychology assessments could advance our understanding of the neural correlates of cognitive and behavioural symptoms in neurodegeneration.

Funding

M.H. is supported by Alzheimer's Research UK, the Wellcome Trust and the Australian Research Council.

Supplementary material

Supplementary material is available at *Brain* online.

References

Baumann O, Borra RJ, Bower JM, Cullen KE, Habas C, Ivry RB, et al. Consensus paper: the role of the cerebellum in perceptual processes. Cerebellum 2014; 14: 197–220.

Beckmann CF, DeLuca M, Devlin JT, Smith SM. Investigations into resting-state connectivity using independent component analysis. Philos Trans R Soc Lond B Biol Sci 2005; 360: 1001–13.

Braak H, Braak E, Bohl J, Lang W. Alzheimer's disease: amyloid plaques in the cerebellum. J Neurol Sci 1989; 93: 277–87.

Braak H, Braak E. Neuropathological stageing of Alzheimer-related changes. Acta Neuropathol 1991; 82: 239–59.

Buckner R, Krienen F, Castellanos A, Diaz JC, Yeo BT. The organization of the human cerebellum estimated by intrinsic functional connectivity. J Neurophysiol 2011; 106: 2322–45.

Buckner RL. The cerebellum and cognitive function: 25 years of insight from anatomy and neuroimaging. Neuron 2013; 80: 807–15.

Chen J, Cohen ML, Lerner AJ, Yang Y, Herrup K. DNA damage and cell cycle events implicate cerebellar dentate nucleus neurons as targets of Alzheimer's disease. Mol Neurodegener 2010; 5: 60

Damoiseaux J. Consistent resting-state networks across healthy subjects. Proc Natl Acad Sci USA 2006; 103: 13848–53.

Dickson DW, Wertkin A, Mattiace LA, Fier E, Kress Y, Davies P, et al. Ubiquitin immunoelectron microscopy of dystrophic neurites in cerebellar senile plaques of Alzheimer's disease. Acta Neuropathol 1990; 79: 486–93.

Diedrichsen J. A spatially unbiased atlas template of the human cerebellum. Neuroimage 2006; 33: 127–38.

Dubois B, Feldman HH, Jacova C, Dekosky ST, Barberger-Gateau P, Cummings J, et al. Research criteria for the diagnosis of Alzheimer's disease: revising the NINCDS-ADRDA criteria. Lancet Neurol 2007; 6: 734–46.

Dubois B, Feldman HH, Jacova C, Hampel H, Molinuevo JL, Blennow K, et al. Advancing research diagnostic criteria for Alzheimer's disease: the IWG-2 criteria. Lancet Neurol 2014; 13: 614–29.

Dukart J, Mueller K, Horstmann A, Vogt B, Frisch S, Barthel H, et al. Differential effects of global and cerebellar normalization on detection and differentiation of dementia in FDG-PET studies. Neuroimage 2010; 49: 1490–5.

Farb NAS, Grady CL, Strother S, Tang-Wai DF, Masellis M, Black S, et al. Abnormal network connectivity in frontotemporal dementia: evidence for prefrontal isolation. Cortex 2013; 49: 1856–73.

Fox MD, Snyder AZ, Vincent JL, Corbetta M, Van Essen DC, Raichle ME. The human brain is intrinsically organized into dynamic, anticorrelated functional networks. Proc Natl Acad Sci USA 2005; 102: 9673–8.

Fukutani Y, Cairns NJ, Rossor MN, Lantos PL. Purkinje cell loss and astrocytosis in the cerebellum in familial and sporadic Alzheimer's disease. Neurosci Lett 1996; 214: 33–6.

Glasser MF, Sotiropoulos SN, Wilson JA, Coalson TS, Fischl B, Andersson JL, et al. The minimal preprocessing pipelines for the Human Connectome Project. Neuroimage 2013; 80: 105–24.

Gorno-Tempini ML, Hillis AE, Weintraub S, Kertesz A, Mendez M, Cappa SF, et al. Classification of primary progressive aphasia and its variants. Neurology 2011; 76: 1006–14.

Greicius MD, Srivastava G, Reiss AL, Menon V. Default-mode network activity distinguishes Alzheimer's disease from healthy aging: evidence from functional MRI. Proc Natl Acad Sci USA 2004; 101: 4637–42.

Guo CC, Gorno-Tempini ML, Gesierich B, Henry M, Trujillo A, Shany-Ur T, et al. Anterior temporal lobe degeneration produces widespread network-driven dysfunction. Brain 2013; 136: 2979–91.

Habas C, Kamdar N, Nguyen D, Prater K, Beckmann CF, Menon V, et al. Distinct cerebellar contributions to intrinsic connectivity networks. J Neurosci 2009; 29: 8586–94.

Haines DE, Dietrichs E, Mihailoff GA, McDonald EF. The cerebellar-hypothalamic axis: basic circuits and clinical observations. Int Rev Neurobiol 1997; 41: 83–107.

Haines DE, Dietrichs E. An HRP study of hypothalamo-cerebellar and cerebello-hypothalamic connections in squirrel monkey (Saimiri sciureus). J Comp Neurol 1984; 229: 559–75.

Ishii K, Sasaki M, Kitagaki H, Yamaji S, Sakamoto S, Matsuda K, et al. Reduction of cerebellar glucose metabolism in advanced Alzheimer's disease. J Nucl Med 1997; 38: 925–8.

Joachim CL, Morris JH, Selkoe DJ. Diffuse senile plaques occur commonly in the cerebellum in Alzheimer's disease. Am J Pathol 1989; 135: 309–19.

Jucker M, Walker LC. Self-propagation of pathogenic protein aggregates in neurodegenerative diseases. Nature 2013; 501: 45–51.

Kelly RM, Strick PL. Cerebellar loops with motor cortex and prefrontal cortex of a nonhuman primate. J Neurosci 2003; 23: 8432–44.

Kipps CM, Davies RR, Mitchell J, Kril JJ, Halliday GM, Hodges JR. Clinical significance of lobar atrophy in frontotemporal dementia: application of an MRI visual rating scale. Dement Geriatr Cogn Disord 2007; 23: 334–42.

Krienen FM, Buckner RL. Segregated fronto-cerebellar circuits revealed by intrinsic functional connectivity. Cereb Cortex 2009; 19: 2485–97.

La Joie R, Perrotin A, De La Sayette V, Egret S, Doeuvre L, Belliard S, et al. Hippocampal subfield volumetry in mild cognitive impairment, Alzheimer's disease and semantic dementia. NeuroImage Clin 2013; 3: 155–62.

Mahoney CJ, Beck J, Rohrer JD, Lashley T, Mok K, Shakespeare T, et al. Frontotemporal dementia with the C9ORF72 hexanucleotide repeat expansion: clinical, neuroanatomical and neuropathological features. Brain 2012; 135: 736–50.

Mattiace LA, Davies P, Yen SH, Dickson DW. Microglia in cerebellar plaques in Alzheimer's disease. Acta Neuropathol 1990; 80: 493–8.

McKhann GM, Knopman DS, Chertkow H, Hyman BT, Jack CR, Kawas CH, et al. The diagnosis of dementia due to Alzheimer's disease: recommendations from the National Institute on Aging-Alzheimer's Association workgroups on diagnostic guidelines for Alzheimer's disease. Alzheimers Dement 2011; 7: 263–9.

Mioshi E, Dawson K, Mitchell J, Arnold R, Hodges JR. The Addenbrooke's Cognitive Examination Revised (ACE-R): a brief cognitive test battery for dementia screening. Int J Geriatr Psychiatry 2006; 21: 1078–85.

Rascovsky K, Hodges JR, Knopman D, Mendez MF, Kramer JH, Neuhaus J, et al. Sensitivity of revised diagnostic criteria for the behavioural variant of frontotemporal dementia. Brain 2011; 134: 2456–77.

Rosen HJ, Gorno-Tempini ML, Goldman WP, Perry RJ, Schuff N, Weiner M, et al. Patterns of brain atrophy in frontotemporal dementia and semantic dementia. Neurology 2002; 58: 198–208.

Salimi-Khorshidi G, Douaud G, Beckmann CF, Glasser MF, Griffanti L, Smith SM. Automatic denoising of functional MRI data: combining independent component analysis and hierarchical fusion of classifiers. Neuroimage 2014; 90: 449–68.

Satterthwaite TD, Elliott MA, Gerraty RT, Ruparel K, Loughead J, Calkins ME, et al. An improved framework for confound regression and filtering for control of motion artifact in the preprocessing of resting-state functional connectivity data. Neuroimage 2013; 64: 240–56.

Scheltens P, Leys D, Barkhof F, Huglo D, Weinstein HC, Vermersch P, et al. Atrophy of medial temporal lobes on MRI in 'probable' Alzheimer's disease and normal ageing: diagnostic value and neuropsychological correlates. J Neurol Neurosurg Psychiatry 1992; 55: 967–72.

Schmahmann JD, Sherman JC. The cerebellar cognitive affective syndrome. Brain 1998; 121: 561–79.

Schmahmann JD. The cerebrocerebellar system: anatomic substrates of the cerebellar contribution to cognition and emotion. Int Rev Psychiatry 2001; 13: 247–60.

Seeley WW, Crawford RK, Zhou J, Miller BL, Greicius MD. Neurodegenerative diseases target large-scale human brain networks. Neuron 2009; 62: 42–52.

Seeley WW, Menon V, Schatzberg AF, Keller J, Glover GH, Kenna H, et al. Dissociable intrinsic connectivity networks for salience processing and executive control. J Neurosci 2007; 27: 2349–56.

Shepherd GMG. Corticostriatal connectivity and its role in disease. Nat Rev Neurosci 2013; 14: 278–91.

Siwek DF, Pandya DN. Prefrontal projections to the mediodorsal nucleus of the thalamus in the rhesus monkey. J Comp Neurol 1991; 312: 509–24.

Smith MA, Richey Harris PL, Sayre LM, Beckman JS, Perry G. Widespread peroxynitrite-mediated damage in Alzheimer's disease. J Neurosci 1997; 17: 2653–7.

Smith SM, Beckmann CF, Andersson J, Auerbach EJ, Bijsterbosch J, Douaud G, et al. Resting-state fMRI in the human connectome project. Neuroimage 2013; 80: 144–68.

Tan RH, Devenney E, Dobson-Stone C, Kwok JB, Hodges JR, Kiernan MC, et al. Cerebellar integrity in the amyotrophic lateral sclerosis-frontotemporal dementia continuum. PLoS One 2014; 9: e105632

Vincent JL, Patel GH, Fox MD, Snyder AZ, Baker JT, Van Essen DC, et al. Intrinsic functional architecture in the anaesthetized monkey brain. Nature 2007; 447: 83–6.

Wedderburn C, Wear H, Brown J, Mason SJ, Barker RA, Hodges J, et al. The utility of the Cambridge Behavioural Inventory in neurodegenerative disease. J Neurol Neurosurg Psychiatry 2008; 79: 500–3.

Wegiel J, Wisniewski HM, Dziewiatkowski J, Badmajew E, Tarnawski M, Reisberg B, et al. Cerebellar atrophy in Alzheimer's disease-clinicopathological correlations. Brain Res 1999; 818: 41–50.

Whitwell JL, Weigand SD, Boeve BF, Senjem ML, Gunter JL, Dejesus-Hernandez M, et al. Neuroimaging signatures of frontotemporal dementia genetics: C9ORF72, tau, progranulin and sporadics. Brain 2012; 135: 794–806.

Yeo BTT, Krienen FM, Sepulcre J, Sabuncu MR, Lashkari D, Hollinshead M, et al. The organization of the human cerebral cortex estimated by intrinsic functional connectivity. J Neurophysiol 2011; 106: 1125–65.

Zhou J, Gennatas ED, Kramer JH, Miller BL, Seeley WW. Predicting regional neurodegeneration from the healthy brain functional connectome. Neuron 2012; 73: 1216–27.

Zhou J, Greicius MD, Gennatas ED, Growdon ME, Jang JY, Rabinovici GD, et al. Divergent network connectivity changes in behavioural variant frontotemporal dementia and Alzheimer's disease. Brain 2010; 133: 1352–67.